EUKARYOTIC CELL, June 2008, p. 1041–1052 Vol. 7, No. 6
1535-9778/08/$08.00+0 doi:10.1128/EC.00071-07

The Nuclear Migration Protein NUDF/LIS1 Forms a Complex with NUDC and BNFA at Spindle Pole Bodies▽

Kerstin Helmstaedt,[1,2] Karen Laubinger,[1,2] Katja Voßkuhl,[1]† Özgür Bayram,[1] Silke Busch,[1]‡ Michael Hoppert,[3] Oliver Valerius,[1] Stephan Seiler,[1,2]* and Gerhard H. Braus[1]*

Molekulare Mikrobiologie und Genetik, Institut für Mikrobiologie und Genetik, Georg-August-Universität Göttingen, Grisebachstraße 8, D-37077 Göttingen, Germany[1]; DFG Research Center for Molecular Physiology of the Brain (CMPB), D-37077 Göttingen, Germany[2]; and Allgemeine Mikrobiologie, Institut für Mikrobiologie und Genetik, Georg-August-Universität Göttingen, Grisebachstraße 8, D-37077 Göttingen, Germany[3]

Received 8 March 2007/Accepted 25 March 2008

Nuclear migration depends on microtubules, the dynein motor complex, and regulatory components like LIS1 and NUDC. We sought to identify new binding partners of the fungal LIS1 homolog NUDF to clarify its function in dynein regulation. We therefore analyzed the association between NUDF and NUDC in *Aspergillus nidulans*. NUDF and NUDC directly interacted in yeast two-hybrid experiments via NUDF's WD40 domain. NUDC-green fluorescent protein (NUDC-GFP) was localized to immobile dots in the cytoplasm and at the hyphal cortex, some of which were spindle pole bodies (SPBs). We showed by bimolecular fluorescence complementation microscopy that NUDC directly interacted with NUDF at SPBs at different stages of the cell cycle. Applying tandem affinity purification, we isolated the NUDF-associated protein BNFA (for *b*inding to *N*UD*F*). BNFA was dispensable for growth and for nuclear migration. GFP-BNFA fusions localized to SPBs at different stages of the cell cycle. This localization depended on NUDF, since the loss of NUDF resulted in the cytoplasmic accumulation of BNFA. BNFA did not bind to NUDC in a yeast two-hybrid assay. These results show that the conserved NUDF and NUDC proteins play a concerted role at SPBs at different stages of the cell cycle and that NUDF recruits additional proteins specifically to the dynein complex at SPBs.

Nuclear movement is a precisely regulated developmental process that is of special importance in highly elongated cells, like neurons or the linear hyphae of filamentous fungi. These cell types grow by apical extension and the subsequent long-range translocation of nuclei into the leading process. In neurons, this nuclear movement can be followed by the retraction of the trailing process so that active cell migration, so-called nucleokinesis, is achieved (37).

Important aspects of nuclear migration were elucidated by genetic analyses performed with the amenable fungal model organism *Aspergillus nidulans*. In a screen for nuclear migration mutant strains, the genes *nudA*, *nudC*, *nudF*, and *nudG* were discovered (60). The human homolog to *nudF* is *Lis1*, the haploinsufficiency of which causes autosomal-dominant lissencephaly type 1 (10). Mutations of *Lis1* lead to retarded neuronal migration to the cerebral cortex, creating disorganized cortical layers. This defective brain development causes mental retardation, epilepsy, and early death. The characterization of LIS1-interacting proteins showed that LIS1 also plays a role in other diseases, like schizophrenia and neuronal degeneration (45). While during the nucleokinesis of neurons a single nucleus is transported through the cytoplasm, fungal growth is characterized by the distribution of multiple nuclei along filamentous hyphae. Mutations of *nudF* prevent the active transport of nuclei out of the spore into the growing hyphae, leading to the accumulation of nuclei near the spore remnant and only incidental nuclear motion, which leads to slow growth and excessive hyphal branching (61). In addition, nuclear migration is important for the development of asexual spores in *A. nidulans*, during which, after several rounds of nuclear division and the budding of specialized cells (sterigmata), uninucleate and green spores are finally released. Without NUDF, mainly anucleate sterigmata are formed, and conidia are generated only if a nucleus occasionally enters a bud (61). Thus, nuclear migration mutants of *A. nidulans* are easily recognized by their knobby, brownish colony appearance due to slow growth and the reduced production of colored spores. NUDF/LIS1 is a 50-kDa dimeric protein with an N-terminal α-helical LisH dimerization motif, a coiled-coil helix, and a C-terminal WD40 domain, which is a β-propeller (29, 53).

The *nudA* and *nudG* nuclear migration mutations of *A. nidulans* that show the same phenotype as the *nudF* mutation affect genes encoding the heavy and light chains, respectively, of the microtubule (MT)-dependent motor dynein (60). NUDF is not a subunit of cytoplasmic dynein, but it regulates dynein motor function. Dynein heavy-chain mutations were isolated as extragenic suppressors of a temperature-sensitive *nudF* mutation (57) and subsequently were shown to affect an ATPase domain of dynein and its stem region (66). NUDF directly bound the first ATPase domain of the dynein heavy chain in a yeast

* Corresponding author. Mailing address: Molekulare Mikrobiologie und Genetik, Institut für Mikrobiologie und Genetik, Georg-August-Universität Göttingen, Grisebachstraße 8, D-37077 Göttingen, Germany. Phone: 49-551-393771. Fax: 49-551-393820. E-mail for S. Seiler: sseiler@gwdg.de. E-mail for G. H. Braus: gbraus@gwdg.de.

† Present address: Abteilung Gastroenterologie, Hepatologie und Endokrinologie, Medizinische Hochschule Hannover, Carl-Neuberg-Straße 1, D-30625 Hannover, Germany.

‡ Present address: Zentrum für Arzneimittelforschung, Entwicklung und Sicherheit (ZAFES), Institut für Klinische Pharmakologie, Klinikum der Johann Wolfgang Goethe-Universität Frankfurt, Theodor-Stern-Kai 7, D-60590 Frankfurt am Main, Germany.

▽ Published ahead of print on 4 April 2008.

two-hybrid analysis (48). Accumulated in vivo data suggest that NUDF is necessary for activating dynein's retrograde transport activity, and without NUDF, dynein accumulates at MT plus ends (63). Dynein heavy chain and NUDF were colocalized at MT plus ends and at spindle poles and influence the stability of MTs by their availability at plus ends (35). Mutations in the encoding genes reduce the frequency of MT catastrophe and rescue events, respectively, indicating that the intact dynein/NUDF complex promotes plus-end dynamics. This is further supported by the isolation of an α-tubulin mutant, which suppresses the *nudA* and *nudF* defects (58). Furthermore, dynein and NUDF regulate the attachment of MT plus ends to the cell cortex; NUDF seems to interact with APSA (for *a*nucleate *p*rimary *s*terigmata *A*), a cortical landmark protein, so that dividing nuclei attached to the MT minus ends can be brought to and fixed at specific cellular positions (56).

In addition, various other *nud* mutants have been described that regulate NUDF function. NUDE is a multicopy suppressor of the *nudF7* mutation and has been shown to interact with NUDF's coiled-coil helix via its own N-terminal coiled-coil domain (13). Its C-terminal domain directs NUDE to MT plus ends, but NUDE also forms immobile specks along hyphae, suggesting additional cortical functions of NUDE (14). Whereas it has been shown that NUDF is recruited to MT plus ends by CLIPA and NUDE (14), it is unknown whether these proteins also are responsible for targeting NUDF to spindle poles. CLIPA belongs to the group of plus-end tracking proteins. The mammalian homolog CLIP-170 also regulates MT dynamics and mediates MT capture at cortical sites (20, 31). Furthermore, NUDF is stabilized by NUDC, and the level of NUDF is reduced in the *nudC3* mutant, indicating that NUDC acts upstream of NUDF (61). In contrast to the other *nud* mutants, a *nudC* deletion in *A. nidulans* results in the loss of polar growth, abnormal cell walls, and the lysis of cells, which hints at additional essential functions (8).

Mammalian NUDC contains an extra N-terminal domain in addition to a conserved p23 domain. Murine NUDC interacts biochemically with LIS1 and copurifies with the dynein heavy and intermediate chains. Similarly, the colocalization of murine NUDC, LIS1, and dynein at MT-organizing centers near the nucleus indicate that NUDC exerts its function at least partly via the regulation of the dynein/LIS1 complex (38). In addition, murine NUDC was found at discrete foci at the cortical cytoskeleton. In different rat cell types, NUDC is localized at the region of the Golgi apparatus (39). Human NUDC (hNUDC) is essential for bipolar spindle formation, indicating a function in MT organization at spindle poles (64). hNUDC also is localized to the kinetochore and regulates MT attachment to chromosomes (41). During late mitosis, it is found at midzone MTs and the midbody in HeLa cells, which emphasizes its role for cytokinesis (1). Thus, NUDC plays a broad role during mitosis, which is in agreement with its high level of expression in proliferating cells. A mitotic function also can be attributed to LIS1. Together with dynein, it is localized at the cell cortex, the centrosome, and mitotic kinetochores, which also regulate spindle orientation, chromosome attachment, and the cortical tethering of astral MTs (16, 52). Unlike the case for *Aspergillus*, *LIS1* overexpression in mammalian cells blocks mitotic progression (16), while the complete inhibition of mitotic entry by the reduction of *LIS1* expression was discussed for nonneural mammalian cells (55).

In this study, we intended to identify new binding partners of the fungal LIS1 homolog NUDF. We analyzed where NUDC is localized in *A. nidulans* and if there are physical interactions between fungal NUDC and NUDF. Furthermore, we asked whether unknown NUDF binding proteins can be identified in this filamentous fungus in order to gain further insights into the molecular function and regulation of this nuclear migration protein.

MATERIALS AND METHODS

Strains, media, and growth conditions. The *Aspergillus nidulans* strains used in this study are listed in Table 1. *Escherichia coli* strains DH5α (59) and SURE (Stratagene, Amsterdam, The Netherlands) were employed for the preparation of plasmid DNA and were grown in Luria-Bertani (LB) medium (1% tryptophan, 0.5% yeast extract, 1% NaCl) in the presence of 100 μg/ml ampicillin. The bacterial strain KS272 carrying the pKOBEG plasmid was grown in LB medium in the presence of 25 μg/ml chloramphenicol (7). Minimal medium (MM; 1% glucose, 2 mM $MgSO_4$, 70 mM $NaNO_3$, 7 mM KCl, 11.2 mM KH_2PO_4, 0.1% trace element solution [28], pH 5.5, 2% agar) and YAG medium (2% glucose, 0.5% yeast extract, 2% agar) either with or without 0.6 mM KCl were used for the growth of *Aspergillus* strains and were supplemented with the appropriate amounts of pyridoxine-HCl (0.1%), uridine (5 mM), and uracil (5 mM) for agar plates. For two-hybrid experiments, *Saccharomyces cerevisiae* strain EGY48 (*MAT*α *trp1 his3 ura3 lexAops-LEU2*) harboring pRB1840 (*URA3 lexAop-lacZ*; 2μ; Ap^r) (22) was grown on selective synthetic complete (SC) medium [0.15% yeast nitrogen base, 0.55% $(NH4)_2SO_4$, 0.1% (vol/vol) 200 mM *myo*-inositol, 0.2% amino acid mix-4, 2% glucose, 2% agar] lacking tryptophan, uracil, histidine, and, in the case of growth assays, leucine (SC-3 and SC-4). When needed, supplements were added according to Guthrie and Fink (24).

Transformation procedures. *E. coli* cells were transformed as described previously (27) or by applying electroporation (50) with a Bio-Rad Gene Pulser at 2.5 kV in 0.2-cm cuvettes (Bio-Rad Laboratories GmbH, München, Germany). *A. nidulans* was transformed by the polyethylene glycol-mediated fusion of protoplasts as described previously (43). *S. cerevisiae* was transformed by a modified method based on that of Elble (15).

Plasmid and strain constructions for TAP. A Δ*nudF* strain was generated for the reintegration of a tandem affinity purification (TAP)-tagged *nudF* version for expression from the authentic promoter. For that purpose, a deletion cassette containing 250-bp 5′-untranslated region (5′ UTR) and 3′ UTR fragments of *nudF* was generated as described by Krappmann et al. (32) using the *zeo*-A*fpyrG*-*zeo* deletion cassette for targeted gene replacement. A 10-kb genomic BglII fragment containing *nudF* was isolated from an *Aspergillus* bacterial artificial chromosome library by using a 640-bp probe, which was amplified using the HexaLabel DNA labeling kit (Fermentas GmbH, St. Leon-Rot, Germany) and hybridized to the 5′ UTR of *nudF*. The genomic fragment was subcloned into BamHI-digested pBluescript (pME2822). This plasmid and the *nudF* deletion cassette were transformed into *E. coli* KS272, and the plasmid resulting from homologous recombination (pME3231) was rescued from KS272. It contained the *nudF*::*zeo*::*pyrG*::*zeo* deletion cassette with a 6-kb 5′ UTR and 3-kb 3′ UTR and was linearized by NotI digestion prior to transformation into *A. nidulans* strain AGB152, yielding strain AGB257 (Δ*nudF*::*zeo*::A*fpyrG*::*zeo pyrG89 pyroA4*). Transformants were selected on YAG medium containing pyridoxine-HCl and 0.6 M KCl and were tested for their lack of nuclear migration by the staining of nuclei, which was performed as described previously (60), and for small-colony growth by growth tests on MM pyridoxine plates and was compared to that of the parental strain. The *pyrG* marker of AGB257 was rescued by being plated on 5-fluoroorotic acid (5-FOA) medium according to Krappmann et al. (32), resulting in strain AGB294.

A TAP-tagged version of *nudF* was reintegrated into the *nudF* locus of AGB257. An MluI site was created 5′ of the start codon of *nudF* in pME2822, which was employed for the integration of the N-terminal TAP tag with optimized codons and without an internal MluI site (*ntap**; pME3232). This plasmid was digested with NotI and transformed into AGB257 with selection on MM containing sorbitol, pyridoxine-HCl, uracil, uridine, and 1 mg/ml 5-FOA, resulting in strain AGB249 (*nTAP**::*nudF pyrG89 pyroA4*). Again, transformants were controlled by the microscopic analysis of nuclear migration and by growth tests, which proved the functionality of the tagged NUDF.

TABLE 1. *Aspergillus nidulans* strains used in this study

Strain	Genotype	Source or reference
AGB152	*pyroA4 pyrG89*	5
A1149	*pyroA4 pyrG89 ΔnkuA::argB*	40
A779	*nudC3 wA2 nicA2 pabaA1 pyrG89*	FGSC (Kansas City, MO)
XX20	*nudF6 pyrG89*	61
AGB241	*pabaA1 nicA2 wA2 pyrG89/pyr-4 nudC3 ^{p}alcA::nudC::sgfp*	This study
AGB249	*nTAP*::nudF pyrG89 pyroA4*	This study
AGB257	*pyroA4 pyrG89 ΔnudF::zeo::pryG::zeo*	This study
AGB294	*pyroA4 pyrG89 ΔnudF::zeo*	This study
AGB295	*pyroA4 pyrG89 ΔnkuA::argB ΔbnfA::zeo*	This study
AGB296	*pyroA4 pyrG89 ΔbnfA::zeo*	This study
AGB297	*pyroA4 pyrG89/pyr-4 ΔbnfA::zeo ^{p}gpdA::nat^{R} ^{p}alcA::gfp2-5::bnfA ^{p}gpdA::mrfp::h2A*	This study
AGB298	*pyrG89/pyr-4 nudF6 ^{p}gpdA::nat^{R} ^{p}alcA::gfp2-5::bnfA ^{p}gpdA::mrfp::h2A*	This study
AGB299	*pyroA4 pyrG89/pyr-4 ΔnudF::zeo ^{p}gpdA::nat^{R} ^{p}alcA::gfp2-5::bnfA ^{p}gpdA::mrfp::h2A*	This study
AGB300	*pyroA4 pyrG89/pyr-4 ΔbnfA::zeo ^{p}alcA::gfp2-5::nudF ^{p}alcA::cfp::tubA*	This study
AGB301	*pyroA4 pyrG89/pyr-4 ^{p}alcA::gfp2-5::nudF ^{p}alcA::cfp::tubA*	This study
AGB302	*pabaA1 nicA2 wA2 pyrG89/*Af*pyrG nudC3 ^{p}niiA::nudF::neyfp ^{p}niaD::nudC::ceyfp*	This study
AGB303	*pyrG89/*Af*pyrG nudF6 ^{p}gpdA::nat^{R} ^{p}niiA::nudF::neyfp ^{p}niaD::nudC::ceyfp ^{p}gpdA::mrfp::h2A*	This study
AGB334	*pyrG89/*Af*pyrG nudF6 ^{p}niiA::nudF::neyfp ^{p}niaD::nudC::ceyfp*	This study
AGB335	*pyrG89/*Af*pyrG nudF6 ^{p}niiA::nudF::neyfp ^{p}niaD::nudC::ceyfp mipA::mrfp::^{p}gpdA::nat^{R}*	This study
AGB336	*pyroA4 pyrG89 ΔnkuA::argB mipA::mrfp::^{p}gpdA::nat^{R}*	This study
AGB337	*pyroA4 pyrG89 ΔnkuA::argB mipA::mrfp::^{p}gpdA::nat^{R} bnfA::gfp2-5::*Af*pyrG*	This study
AGB338	*pyroA4 pyrG89/pyr-4 ΔnkuA::argB mipA::mrfp::^{p}gpdA::nat^{R} nudC::gfp2-5::^{p}alcA::nudC*	This study

Plasmid and strain constructions for *bnfA* deletion. The *bnfA* knockout strain was generated by applying the *zeo*-Af*pyrG-zeo* deletion cassette. A 998-bp 5′ UTR and a 976-bp 3′ UTR fragment were PCR amplified and cloned into the EcoRV and HpaI restriction sites of pME2409, respectively (OLKH241, 5′-ATC GTG ATT CTC TAT TGG ATC TCG-3′; OLKH242, 5′-GGA GCT GGC TGG AGA TCG-3′; OLKH243, 5′-GAC TCG CGA TAA GAG TAC AC-3′; and OLKH244, 5′-AAC CTG TTT CAT TGG ACC CGT AG-3′), resulting in plasmid pME3233. The linearized plasmid was transformed into the Δ*nkuA* strain A1149, and transformants were selected on YAG medium containing pyridoxine-HCl and 0.6 M KCl. The *pyrG* marker was rescued by being plated on 5-FOA medium, resulting in strain AGB295. Since the backcrossing of these Δ*nkuA* strains was not successful, the Δ*bnfA*::*zeo* deletion also was generated in the AGB152 strain background (AGB296), and the last one was used for localization experiments.

Plasmid and strain constructions for localization experiments. NUDC-green fluorescent protein (NUDC-GFP) was localized in an *A. nidulans nudC3* strain after the transformation of pME2823 harboring a *nudC*::*sgfp* fusion into A779 (AGB241). pME2823 was created by cloning a KpnI fragment of *nudC* into pMCB32 (18) (OLKH115, 5′-AAG GTA CCA TGT CGG AAC AAG AAC CGT C-3′; and OLKH116, 5′-AAG GTA CCC CAA TCT TCG CAT TCG AAA AG-3′).

For the colocalization of NUDF and NUDC, the encoding genes were fused to the N-terminal and C-terminal halves of enhanced YFP (eYFP), respectively, by fusion PCR and were cloned into the blunt PmeI and SwaI sites, respectively, of plasmid pME3160, which contains the bidirectional *niiA*/*niaD* promoter. For PCR, template plasmids pME3012 and pME3013 (4) and pME2822/pME2823 as well as the following primers, encoding an RSIAT linker for the *nudF*::*neyfp* fusion and an RPACKIPNDLKQKVMNH linker between NUDC and cEYFP, were used: OLKH262, 5′-ATG AGC CAA ATA TTG ACA GCT C-3′; OLKH263, 5′-CTC CTC GCC CTT GCT CAC CGT GGC GAT GGA GCG GCT GAA CAC CCG TAC AGA G-3′; OLKH264, 5′-CTC TGT ACG GGT GTT CAG CCG CTC CAT CGC CAC GGT GAG CAA GGG CGA GGA GCT G-3′; OLKH265, 5′-TTA GAT ATA GAC GTT GTG GCT GTT GTA G-3′; OLKH258, 5′-ATG TCG GAA CAA GAA CCG TC-3′; OLKH259, 5′-GTG GTT CAT GAC CTT CTG TTT CAG GTC GTT CGG GAT CTT GCA GGC CGG GCG ACC AAT CTT CGC ATT CGA AAA GTC-3′; OLKH260, 5′-CGC CCG GCC TGC AAG ATC CCG AAC GAC CTG AAA CAG AAG GTC ATG AAC CAC GCC GAC AAG CAG AAG AAC GGC ATC AAG-3′; and OLKH261, 5′-TTA CTT GTA CAG CTC GTC CAT GCC GAG AGT GAT CCC-3′. The resulting plasmid, pME3238, was transformed into A779 and XX20 to test for the complementation of their temperature-sensitive phenotypes at 42°C, yielding strains AGB302 and AGB334. AGB334 also was transformed with pME3173, expressing the nuclear marker ^{p}*gpdA*::*mrfp*::*h2A* (S. Krappmann, personal communication), resulting in strain AGB303. For colocalization with γ-tubulin, AGB334 was transformed with a PCR product comprising a *mipA*::*mrfp*::^{p}*gpdA*::*nat*^{R} cassette (AGB335). For this fusion PCR, a template plasmid was generated: a $(GA)_5$ linker, the *mrfp* gene, and the *nat*^{R} expression module were amplified with primers OLKH301 (5′-GGA ATT CGG AGC TGG TGC AGG CGC TGG AGC CGG TGC CGC CTC CTC CGA GGA CGT C-3′), OLKH302 (5′-ACC GGT CAC TGT ACA GAG CTG CGG CCG CTT AGG CGC CGG TGG AGT GG-3′), OLKH303 (5′-CCA CTC CAC CGG CGC CTA AGC GGC CGC AGC TCT GTA CAG TGA CCG GT-3′), and OLKH304 (5′-CGG GAT CCT CAG GGG CAG GGC ATG CTC-3′) and were cloned into pBluescript via EcoRI/BamHI, yielding plasmid pME2984. This module (OLKH306, 5′-GGA GCT GGT GCA GGC GCT G-3′; and OLKH307, 5′-TCA GGG GCA GGG CAT GCT C-3′) was fused to a 500-bp homology region that included a part of *mipA* (OLKH308, 5′-GCA TGA ACG ACC GAT TTC CG-3′; and OLKH310, 5′-TCC AGC GCC TGC ACC AGC TCC TAC TCC AAC TTC ATC CTT TCC-3′) and a 500-bp region comprising the 3′ UTR of *mipA* (OLKH311, 5′-GAG CAT GCC CTG CCC CTG AAT TCA GCC TAG ATA TAA TGT ACC-3′; and OLKH313, 5′-CAT TGA TAG GAA CAG GTG ACT TG-3′), which were amplified using genomic DNA by a final fusion PCR with OLKH309 (5′-GCA GAT GTC GTG GTC AAC C-3′) and OLKH312 (5′-CCC AAT CCC CTG GTT GAG AC-3′).

A *gfp*::*bnfA* fusion was expressed in the Δ*bnfA* strain. For that purpose, an AscI/PacI fragment of the *bnfA* open reading frame (ORF) was cloned into pMCB17apx (OLKH246, 5′-AGG CGC GCC CGC CCC CGT CAA GTT CAC CAA G-3′; and OLKH247, 5′-CCT TAA TTA ATC ATG TTT CCT TTG CCT CAG-3′), and the resulting plasmid, pME3234, was transformed into AGB296 together with pME3173 for the expression of the nuclear marker ^{p}*gpdA*::*mrfp*::*h2A*, yielding strain AGB297. The same plasmids were transformed into strains XX20 and AGB294, resulting in strains AGB298 and AGB299.

In order to rule out overexpression effects, a *bnfA*::*gfp* fusion was expressed from the authentic *bnfA* promoter in strain AGB337. For this purpose, a Δ*nkuA* strain was transformed with a PCR product comprising *bnfA*::*gfp2-5*::Af*pyrG* (AGB337). This module was generated by fusion PCR (OLKH342, 5′-GGT TTG TCC TCG TCT ATA CTG-3′; and OLKH344, 5′-CGT CTT TCG GCA TAT ACC AG-3′) covering a 2.5-kb homology region that included the 5′ UTR and the *bnfA* ORF (OLKH341, 5′-GAG CCT GTC GGC GTC ACG-3′; and OLKH317, 5′-TCC AGC GCC TGC ACC AGC TCC TGT TTC CTT TGC CTC AGT CTG-3′), a $(GA)_5$ linker, the *gfp2-5* gene, Af*pyrG* (OLKH306, 5′-GGA GCT GGT GCA GGC GCT G-3′; and OLKH314, 5′-CTG TCT GAG AGG AGG CAC TG-3′), and a 2.2-kb homology region with the 3′ UTR of *bnfA* (OLKH343, 5′-CAG TGC CTC CTC TCA GAC AGC AGG GAG TCG ACT CGC GA-3′; and OLKH345, 5′-GAT TAC GCC TTC CCA GTC ATG-3′), for which genomic DNA and plasmid pFNO3 (62), respectively, served as templates. Furthermore, strain AGB337 harbored the *mipA*::*mrfp*::^{p}*gpdA*::*nat*^{R} cassette, which previously was introduced into A1149 (AGB336).

To rule out overexpression effects when localizing the *nudC-gfp* fusion, we also transformed strain AGB336 with pME2985, which was generated by cloning a

KpnI fragment with *nudC* into a pMCB17apx derivative (pME3322). In some transformants, this plasmid did not integrate ectopically but did so solely at the *nudC* locus, resulting in a *gfp2-5*-labeled *nudC* copy driven by the authentic promoter and an unlabeled copy driven by the *alcA* promoter from the plasmid. Therefore, this strain (AGB338) was grown in glucose medium for microscopic analysis so that no unlabeled NUDC was present in the cells.

For the localization of NUDF in the Δ*bnfA* strain, *nudF* was cloned into pMCB17apx via AscI/PacI (OLKH272, 5′-AGG CGC GCC CAG CCA AAT ATT GAC AGC TCC-3′; and OLKH273, 5′-CCT TAA TTA ATT AGC TGA ACA CCC GTA CAG-3′), and a *cfp-h2A* plasmid (51a) was used to exchange *h2A* against a NotI/SmaI fragment with *tubA* (OLKH274, 5′-CTA AGA ATG CGG CCG CAG AGA AGT CAT TAG TTT GAA CG-3′; and OLKH275, 5′-GCC CCC GGG TTA GTA CTC AAC TTC CTC ACC-3′). The resulting plasmids, pME3235 and pME3236, were transformed into AGB296 and AG152 as a control, yielding strains AGB300 and AGB301.

All ORFs were amplified using *Pfu* (Stratagene, Amsterdam, The Netherlands), KOD Hifi DNA polymerases (Novagen/Merck Chemicals Ltd., Bad Soden am Taunus, Germany), or Phusion high-fidelity DNA polymerase (Finnzymes/New England Biolabs GmbH, Frankfurt am Main, Germany) and were sequenced on an ABI Prism 310 capillary sequencer (Applera Deutschland GmbH, Darmstadt, Germany). Fungal genomic DNA was prepared as described previously (30), and Southern analyses of all strains were carried out according to Southern (51).

TAP and protein identification by tandem mass spectrometry. TAP was performed by the modified method of Busch et al. (6). For the preparation of crude extracts, 45 g of dried vegetative mycelia of strains AGB152 and AGB249 were incubated with buffer B containing 300 mM NaCl (100 mM Tris-HCl, pH 7.2, 300 mM NaCl, 10% glycerol, 0.1% NP-40, 1 mM dithiothreitol [DTT], 14.3 mM β-mercaptoethanol) to disassociate NUDF from MTs. Crude extracts were dialyzed against 2 liters of buffer D (20 mM K-HEPES, pH 7.9, 50 mM KCl, 0.2 mM EDTA, pH 8.0, 0.5 mM DTT, 20% glycerol, 0.5 mM phenylmethylsulfonyl fluoride [PMSF], 2 mM benzamidine) for 3 h and then adjusted to 10 mM Tris-Cl, pH 8.0, 150 mM NaCl, and 0.1% NP-40. Immunoglobulin G (IgG) Sepharose 6 Fast Flow beads (200 μl; Amersham Biosciences/GE Healthcare, München, Germany) were washed with 5 ml of IPP150 (25 mM Tris-HCl, pH 8.0, 150 mM NaCl, 0.1% NP-40) and incubated with 50 ml of crude extract on a rotating platform for 12 h. The suspension was poured into a Bio-Rad PolyPrep column (Bio-Rad Laboratories, GmbH, München, Germany), in which beads were washed twice with 10 ml of IPP300 (25 mM Tris-HCl, pH 8.0, 300 mM NaCl, 0.1% NP-40), with 10 ml of IPP150, and with 10 ml of tobacco etch virus (TEV) cleavage buffer (25 mM Tris-HCl, pH 8.0, 150 mM NaCl, 0.1% NP-40, 0.5 mM EDTA, 1 mM DTT). The following protease inhibitors were added to buffer B, IPP300, and IPP150: 5 μl 1 M DTT, 50 μl 0.1 M PMSF, 40 μl 0.5 M benzamidine, 5 μl leupeptin (1 mg/ml), 10 μl pepstatin (1.4 mg/ml), 12 μl chymostatin (2 mg/ml), and 100 μl aprotinin (1.7 mg/ml) per 10 ml of buffer. In the sealed column, beads were incubated with 1 ml of TEV cleavage buffer containing 300 U TEV protease on a rotating platform for 4 h. Proteins cleaved from the beads were eluted into a Falcon tube, and elution was repeated with another milliliter of TEV cleavage buffer. After the addition of 6 ml calmodulin binding buffer (CBB; 25 mM Tris-HCl, pH 8.0, 150 mM NaCl, 1 mM Mg acetate, 1 mM imidazole, 2 mM $CaCl_2$, 10 mM β-mercaptoethanol) and 6 μl of 1 M $CaCl_2$, the solution was incubated with 200 μl of calmodulin beads (Stratagene, Amsterdam, The Netherlands) on a rotating platform for 4 h. The calmodulin beads were equilibrated with 5 ml of CBB prior to incubation and were washed twice with 1 ml of CBB containing 0.1% NP-40 and with 1 ml of CBB containing 0.02% NP-40. Proteins were eluted with 2 ml of calmodulin elution buffer (25 mM Tris-HCl, pH 8.0, 150 mM NaCl, 0.02% NP-40, 1 mM Mg acetate, 1 mM imidazole, 20 mM EGTA, 10 mM β-mercaptoethanol). The final eluate was precipitated by trichloroacetic acid (TCA), including the adjustment of aliquots to 25% TCA, incubation on ice for 30 min, centrifugation at 4°C in a Microfuge for 30 min, and two washes with cold acetone. After being dried in a speed vacuum, the pellet was resuspended in protein loading dye. After separation on a polyacrylamide gel (34), protein bands were silver stained (3) and cut out. Excised polyacrylamide gel pieces of protein bands were digested with trypsin according to Shevchenko et al. (49). Peptides then were separated by water-acetonitrile gradients on a Dionex-NAN75-15-03-C18-PM column on an ultimate-nano-HPLC system (Dionex, Idstein, Germany). Online ESI-MS/MS2 spectra were generated on an LCQ-DecaXP^{plus} mass spectrometer (Thermo Finnigan/Thermo Scientific, Dreieich, Germany). MS2 analysis and protein diagnosis was done with the software SEQUEST/TURBOSEQUEST (Bioworks Browser 3.1; Thermo Finnigan) by using the Broad Institute public *A. nidulans* genome protein database (http://www.broad.mit.edu/annotation/genome/aspergillus_nidulans/Home.html).

A Western hybridization with a rabbit anti-calmodulin binding peptide antibody (Upstate/Millipore GmbH, Schwalbach, Germany) was performed with samples taken during the purification procedure, which were transferred to a nitrocellulose membrane by being electroblotted after sodium dodecyl sulfate-polyacrylamide gel electrophoresis (SDS-PAGE) and were detected by the enhanced chemiluminescence method (54).

Yeast two-hybrid analysis. Protein-protein interactions were tested by applying the interaction trap of Golemis et al. (22). In this system, plasmids pEG202 and pJG4-5 were used for the expression of ORFs encoding bait and prey proteins and for the activation of *lacZ* and *leu2* reporter constructs to discriminate on the basis of color in the presence of 5-bromo-4-chloro-3-indolyl-β-D-galactopyranoside (X-Gal) or to select for viability on medium lacking leucine. The complete ORF of *nudF* was PCR amplified from the sexual cDNA library pCNS4 (33), with specific primers containing flanking NcoI and XhoI sites, and was cloned into pEG202 (OLKH146, 5′-CAT CCA TGG ATG AG CCA AAT ATT GAC AGC TC-3′; and OLKH147, 5′-CCC CTC GAG TTA GCT GAA CAC CCG TAC AGA-3′; pME2938). *nudF* also was cloned into pJG4-5 as an XhoI fragment (OLKH226, 5′-CGC CTC GAG AGC CAA ATA TTG ACA GCT CC-3′; and OLKH147, 5′-CCC CTC GAG TTA GCT GAA CAC CCG TAC AGA-3′; pME3237). The *nudC* ORF was amplified using OLKH148 (5′-CG GAA TTC ATG TCG GAA CAA GAA CCG TC-3′) and OLKH149 (5′-CG GAA TTC CTA ACC AAT CTT CGC ATT CG-3′) and was cloned into pJG4-5 and pEG202, respectively, as EcoRI fragments (pME3245 and pME3246). The 1,065-bp cDNA encoding BNFA (for *b*inding to *NUDF*) was PCR amplified and inserted as an EcoRI/XhoI fragment into pJG4-5 and pEG202 (OLKH194, 5′-CG GAA TTC ATG GCG ATG GCC CCC GTC-3′; and OLKH195, 5′-CCG CTC GAG TCA TGT TTC CTT TGCC TCA GTC-3′; pME3239 and pME3240). As a positive control, the first 585 bp encoding the coiled-coil region of NUDE were PCR amplified and cloned as an EcoRI/XhoI fragment into pJG4-5 (OLKH162, 5′-CG GAA TTC ATG CCT TCC GCC GAT GAG C-3′; and OLKH163, 5′-CCC CTC GAG GTT ATT GTT CCT GAG CCT CTC-3′; pME2939). As a negative control, vector pME2938 was used in combination with empty vector pJG4-5.

For the domain interaction analysis, the LisH motif/coiled-coil region of *nudF* (amino acids [aa] 1 to 100) was amplified with primers OLKM3 (5′-CCC CTC GAG ATG AGC CAA ATA TTG ACA GCT C-3′) and OLKM15 (5′-CCC CTC GAG TTA CCA ATT GGT CGG ATC TTG G-3′) and cloned into pJG4-5 and pEG202, respectively, via XhoI (pME3241 and pME3242). The region encoding the WD40 domain of *nudF* (aa 99 to 445) was amplified using primers OLKM5 (5′-CCC CTC GAG AAT TGG CTT CCT AAA CCG TC-3′) and OLKH147 and was cloned as an XhoI fragment into both vectors (pME3243 and pME3244). The 5′ part of *nudC*, encoding aa 1 to 28, was amplified with OLKH148 and OLKM12 (5′-CG GAA TTC TTA CTC AGC TTC TTC GGC GGC-3′) and was cloned as an EcoRI fragment (pME3247 and pME3248). The region for the p23 domain (aa 29 to 116) was amplified using OLKM8 (5′-CG GAA TTC CAG GCG ACC CTC CCC TAC-3′) and OLKM13 (5′-CG GAA TTC TTA GTT GAC TTT GTC AAG GTG GAT G-3′) and was cloned as an EcoRI fragment (pME3249 and pME3250), and the C-terminal part (aa 117 to 199) was generated using OLKM10 (5′-CG GAA TTC CAG ATG GAG TGG TGG GC-3′) and OLKM14 (5′-CG GAA TTC TTA ACC AAT CTT CGC ATT CGA AAA G-3′) and also was cloned as an EcoRI fragment (pME3251 and pME3252).

All ORFs were amplified using *Pfu* or KOD Hifi DNA polymerases and were sequenced on an ABI Prism 310 capillary sequencer. The constructs were transformed in different combinations into strain EGY48(pRB1840).

Western hybridization experiments were performed for expression analysis using anti-hemagglutinin (Sigma-Aldrich Chemie GmbH, Munich, Germany) and anti-LexA antibodies (Santa Cruz Biotechnology, Inc., Heidelberg, Germany), respectively.

For interaction tests, overnight SC cultures were diluted to an optical density at 546 nm of 0.2 with SC medium, and 10 μl of the dilution was dropped onto SC-4 plates containing either 2% galactose–1% raffinose or 2% glucose (negative control) for growth tests. Dilutions at an optical density at 546 nm of 0.1 were spotted onto SC-3 plates containing 2% galactose–1% raffinose and 1.7 mM leucine for subsequent β-galactosidase filter assays. Plates were incubated at 30°C for 2 days. For the filter assay, a Whatman filter was placed onto the yeast plate, shock frozen in liquid nitrogen, and dried. The filter then was put onto another Whatman filter soaked with 3 ml of Z buffer (60 mM Na_2HPO_4, 40 mM NaH_2PO_4, 10 mM KCl, 1 mM $MgSO_4$, 0.1% X-Gal) and incubated at 30°C for 4 h.

Microscopy. Five hundred microliters of the appropriate medium was put onto coverslips, which were placed in petri dishes and inoculated with 4×10^4 spores. For growth at 42°C, coverslips were placed into 6-well plates with 5 ml of medium

inoculated with 2×10^5 spores or into petri dishes with 20 ml of medium inoculated with 1×10^6 spores. After incubation at the respective temperatures, slides were mounted on glass slides with nail polish. For the staining of nuclei, 1 μl of 4′,6′-diamidino-2-phenylindole (DAPI) was spotted onto the glass slide before placing the coverslip onto it. Cells were examined with a Zeiss 100 Axiovert microscope (Carl Zeiss MicroImaging GmbH, Jena, Germany), and photographs were taken using a Xillix Microimager digital camera (Xilix Technologies Corp., Richmond, Canada) and the Openlab software (Improvision, Coventry, United Kingdom).

For electron microscopy, embedding in Lowicryl K4M resin was performed as described previously (26, 46). Resin sections of about 80 nm in thickness were cut with glass knives. The sections were stained for 3 min with 3% [wt/vol] phosphotungstic acid solution, pH 7.0. Specimens were analyzed with a Philips EM 301 instrument (Philips, Hamburg, Germany) at calibrated magnifications and using IMAGO electron-sensitive films (Atomic Force F&E GmbH, Mannheim, Germany). Immunogold labeling was performed as described earlier (26).

In silico analyses. For manual annotations, we used the genome databases of CADRE (www.cadre-genomes.org.uk), TIGR (www.tigr.org/tdb/e2k1/afu1/), the Broad Institute (www.broad.mit.edu/annotation/fungi/fgi/), JGI (genome.jgi-psf.org), and the Center for Integrated Fungal Research (www.aspergillusflavus.org). Domain analyses were performed using MyHits (myhits.isb-sib.ch/cgi-bin/motif_scan) and the COILS server (www.ch.embnet.org/software/COILS_form.html). Protein alignments were carried out with NPSA (npsa-pbil.ibcp.fr/cgi-bin/npsa_automat.pl?page=npsa_clustalw.html).

RESULTS

NUDC is localized to immobile dots at the cell cortex. Mammalian NUDC was described to interact and colocalize with LIS1, while fungal NUDC was only shown to stabilize NUDF posttranslationally (61). Therefore, we intended to characterize the fungal NUDC in more detail. As a first step toward deciphering its molecular function, we localized NUDC in *A. nidulans*. We expressed a *^{p}alcA*::*nudC*::*sgfp* fusion in the *nudC3* strain (AGB241) and confirmed the functionality of the fusion protein by the complementation of the temperature-sensitive *nudC3* phenotype by growing AGB241 at 42°C (data not shown). Fluorescence microscopy was performed after the germination of spores in glycerol-containing medium at 42°C. NUDC-GFP was observed as immobile dots along hyphae that were obviously near the cytoplasmic membrane (Fig. 1A). We also conducted immunoelectron microscopy for a more detailed view of the NUDC-GFP position. In fact, NUDC-GFP was detected at the hyphal cortex, with isolated spots in the cytoplasm (Fig. 1B). In the enlarged tip section, NUDC also decorated the cortex around the hyphal tip. Thus, the majority of NUDC obviously localized differently from NUDF, which was detected at spindle poles and MT plus ends, but rather resembled the immobile specks observed for NUDE (12).

NUDF associates with NUDC at spindle pole bodies (SPBs) and at the cortex. Although at first sight NUDF and NUDC localized at different sites in *A. nidulans*, the colocalization of their homologs in mammalian cells prompted us to pursue the investigation of the putative interaction between the *Aspergillus* proteins. We analyzed their association in a yeast two-hybrid assay based on LexA and B42 fusions, respectively. The B42-NUDC fusion protein was not correctly expressed, so it could not be detected by Western hybridization (data not shown). The LexA-NUDC fusion was detected by Western hybridization and associated with the B42-NUDF fusion, as indicated by the expression of the *LEU2* and *lacZ* reporter genes (Fig. 2B). Furthermore, we wanted to specify by which domains of NUDF and NUDC the attachment is accomplished. Based on analyses with computer programs and its

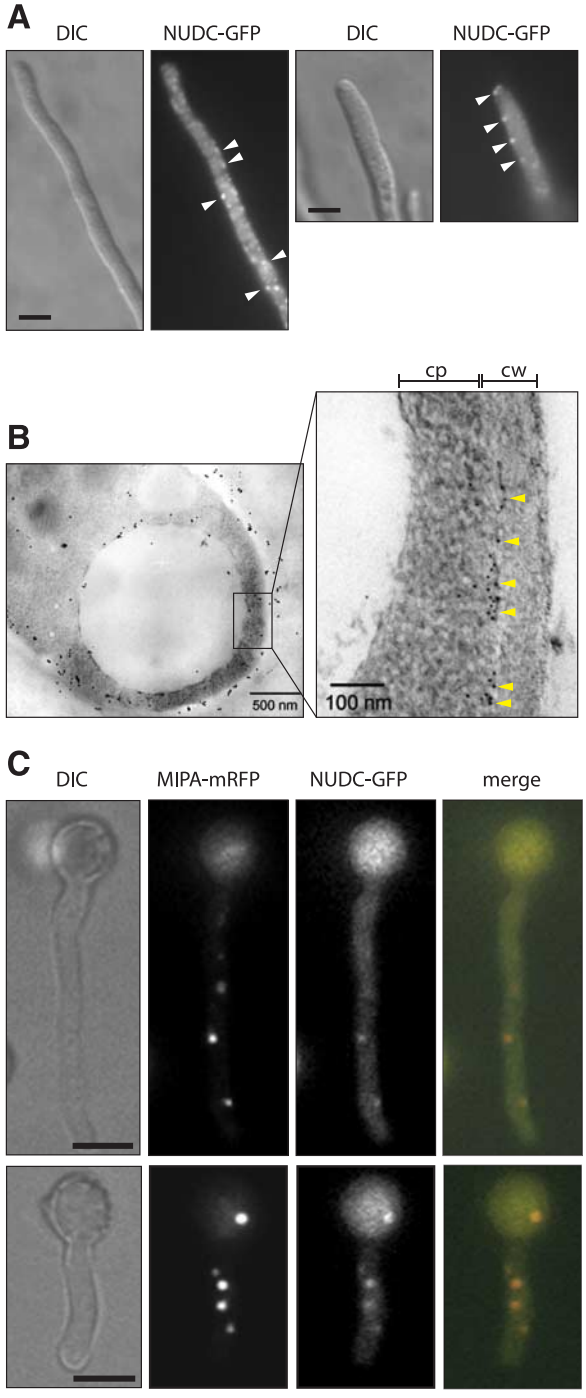

FIG. 1. NUDC is localized to immobile dots at the *A. nidulans* hyphal cortex. Fluorescence microscopy (A) and immunoelectron microscopy (B) of strain AGB241 showed that NUDC-GFP dots are positioned along the hyphal cortex and the tip (examples are indicated by arrowheads). The strain was grown in MM containing 2% ethanol at 42°C for 15 h. Scale bars in panel A, 2.5 μm. cp, cytoplasm; cw, cell wall. (C) In strain AGB338, NUDC-GFP colocalized with γ-tubulin (MIPA) at SPBs. The strain was grown in glucose-containing MM at room temperature for 8 h. Scale bars, 5 μm. DIC, differential interference contrast.

similarity to p23 (21), NUDC was predicted to consist of an N-terminal coiled-coil helix that replaces a large coiled-coil domain of mammalian NUDC, a p23-like central domain (a β-sandwich), and an unknown C-terminal domain of 83 aa

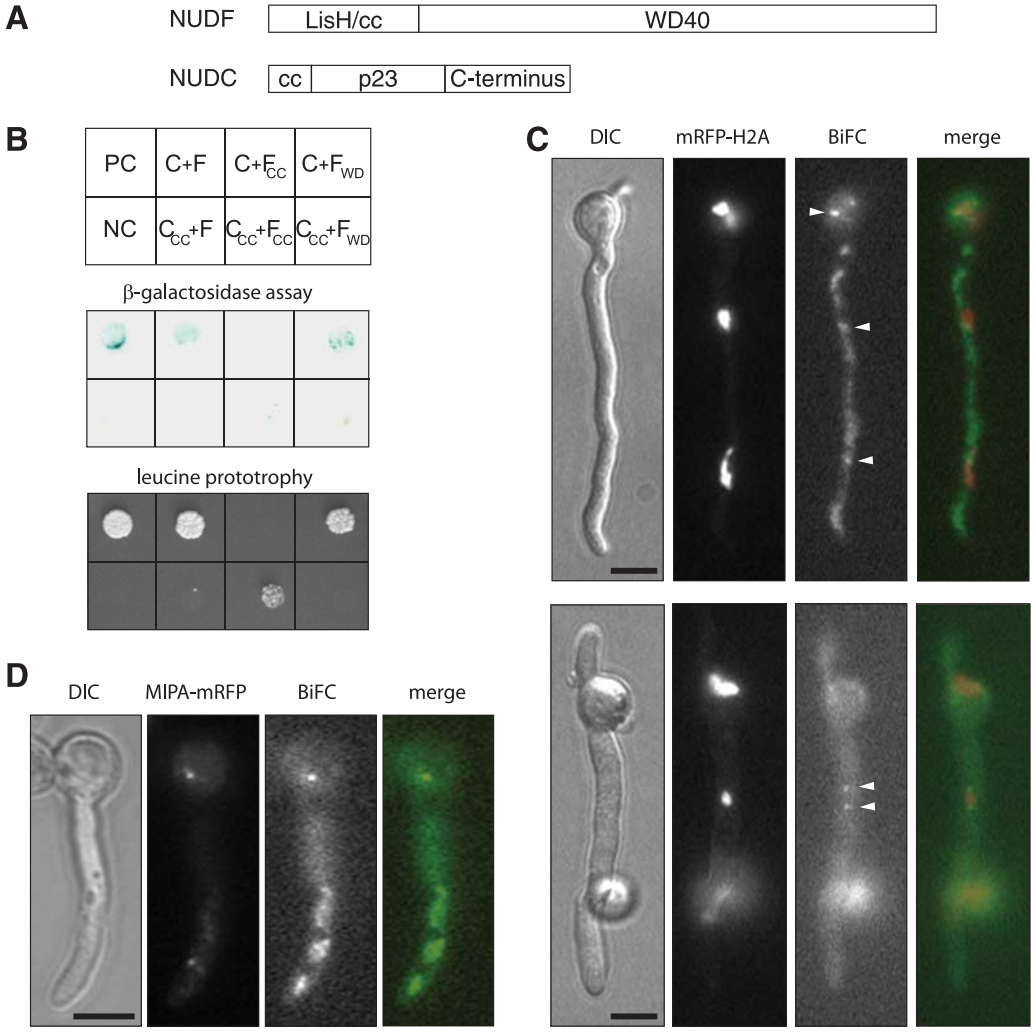

FIG. 2. NUDF binds to NUDC at SPBs via its WD40 domain. (A) NUDF presumably consists of a LisH dimerization motif followed by a coiled-coil helix (cc) and a WD40 domain. NUDC was predicted to form an N-terminal coiled-coil helix, a p23 domain, and a C-terminal domain of unknown structure. (B) In this yeast two-hybrid analysis, LexA-NUDC ("C") interacted with B42-NUDF ("F") and B42-NUDF$_{WD40}$ and induced *LEU2* and *lacZ* reporter gene expression (EGY48 harboring pRB1840, pME3246, and pME3237 and EGY48 harboring pRB1840, pME3246, and pME3243). NUDF binding to the coiled coil of NUDE (EGY48 harboring pRB1840, pME2938, and pME2939) was used as the positive control (PC). NUDF and the empty prey vector (EGY48 harboring pRB1840, pME2938, and pJG4-5) were used as the negative control (NC). CC, coiled coil; WD, WD40 domain. (C) BiFC. Strain AGB303, expressing the *nudF*::*neyfp* and *nudC*::*ceyfp* fusions and the nuclear marker *mrfp*::*h2A*, was cultivated in MM at 42°C for 8 h. The colocalization of NUDF and NUDC was shown through the fluorescence emission, which could be generated only by the colocalization of the N- and C-terminal halves of eYFP (examples are indicated by arrowheads). Scale bars, 5 μm. (D) BiFC. Strain AGB335, expressing the BiFC constructs and the SPB marker *mipA*::*mrfp*, was grown in MM at 42°C for 8 h. Scale bars, 5 μm. DIC, differential interference contrast.

(Fig. 2A). NUDF presumably contains an N-terminal LisH dimerization motif followed by a coiled-coil helix and a large WD40 domain (a β-sheet propeller) (Fig. 2A) (29, 53). The parts of the ORFs encoding these domains were fused to the respective two-hybrid domains and expressed in yeast for comparisons to the full-length ORFs. The growth assay as well as the β-galactosidase filter assay revealed an interaction between the full-length NUDC and the WD40 domain of NUDF (Fig. 2B). In the growth assay, a presumably false-positive interaction was detected between the coiled-coil domains of NUDF and NUDC through the expression of the more sensitive *LEU2* reporter construct. No interactions were observed involving the separate p23 and C-terminal domain of NUDC, respectively, although all fusion proteins were detected by Western hybridization (data not shown). Whether the single domains do not adopt the correct fold when fused to the two-hybrid domains or whether the domains must form a specific quaternary structure that then can bind to NUDF's WD40 domain cannot be resolved at the moment. Thus, using two-hybrid analysis, we could not identify the interacting domain of NUDC.

However, these results made us analyze the NUDF-NUDC interaction in vivo. For that purpose, we constructed fusions with the N-terminal and C-terminal halves of eYFP to observe bimolecular fluorescence complementation (BiFC) in case both fusion proteins were in close contact with each other (25).

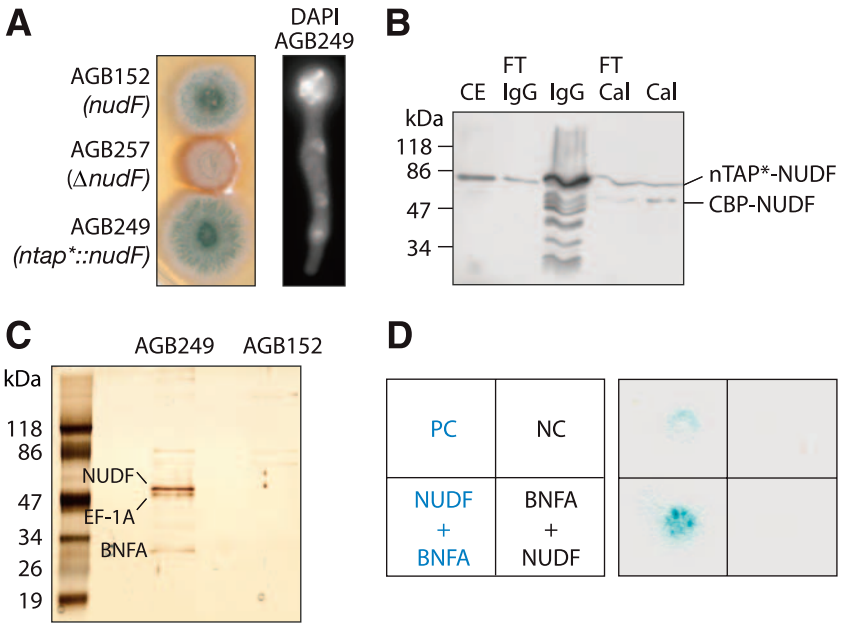

FIG. 3. TAP of proteins binding to *A. nidulans* NUDF. (A) The *ntap**::*nudF* fusion in AGB249 partially complements the nuclear migration defect of the isogenic Δ*nudF* strain AGB257 and restores the growth rate and formation of green conidia, as observed for the parental *nudF* wild-type strain AGB152. (B) The NUDF fusion protein was detected in samples taken during the purification procedure. Twenty micrograms of protein or 5 μl of beads was subjected to SDS-PAGE on a 12% acrylamide gel and hybridized with an anti-calmodulin binding peptide antibody after electroblotting. While the full-length 69-kDa nTAP*-NUDF was detected in the crude extract of AGB249 (CE), in the flowthrough of IgG affinity purification (FT IgG) and on the IgG beads (IgG), the 54-kDa CBP-NUDF was seen after TEV cleavage in a small amount in the flowthrough of the calmodulin affinity purification (FT Cal) and also on the calmodulin beads (Cal). (C) The final eluates of the TAPs performed with crude extracts of AGB249 and of the *nudF* wild-type control strain AGB152 were subjected to SDS-PAGE on a 12% acrylamide gel for silver staining and subsequent identification by mass spectrometry. (D) In a yeast two-hybrid analysis, LexA-NUDF interacted with B42-BNFA and induced *lacZ* reporter gene expression (EGY48 harboring pRB1840, pME2938, and pME3239). The *lexA-bnfA* fusion in strain EGY48 harboring pRB1840, pME3240, and pME323 was not expressed. NUDF binding to the coiled coil of NUDE (EGY48 harboring pRB1840, pME2938, and pME2939) was used as a positive control (PC). NUDF and the empty prey vector (EGY48 harboring pRB1840, pME2938, and pJG4-5) were used as the negative control (NC).

The fusions were expressed from the bidirectional *niiA*/*niaD* promoter by growth on nitrate-containing medium and partially complemented the temperature-sensitive phenotypes when expressed in the *nudC3* and *nudF6* strains (AGB302 and AGB303, respectively). These strains grew faster and produced more conidia than the temperature-sensitive parental strains at 42°C but did not grow as fast at 30°C, which indicated the partial functionality of the NUDF-nEYFP and NUDC-cEYFP fusions (data not shown). Although the YFP emission was low, numerous dots were detected along hyphae and at nuclei that were labeled by the constitutive expression of an *mrfp*::*h2A* fusion (Fig. 2C). Fluorescence also was detected at both poles of mitotic nuclei (Fig. 2C), showing that NUDF-NUDC interaction also takes place at SPBs during mitosis.

These sites were clearly identified as SPBs by colocalization with γ-tubulin (MIPA), which was fused to monomeric RFP (mRFP) in strain AGB335 (Fig. 2D). In this strain, a few prominent spots were observed among several fainter fluorescent spots in the cytoplasm, and the prominent spots clearly could be allocated to the mRFP-labeled SPBs. The SPBs often jerked in the cells but also were found immobilized near the cortex, in which case accurate superimposition with BiFC spots could be best achieved.

To investigate whether some of the dots observed for NUDC-GFP alone also colocalized with SPBs, we introduced a *nudC*::*gfp* fusion into a strain harboring the *mipA*::*mrfp* fusion (AGB338) (Fig. 1C). In addition, *nudC* was not overexpressed but was expressed from the authentic promoter, and it was fused to the more stable *gfp2-5* version. In fact, NUDC-GFP spots could be colocalized with MIPA-mRFP signals even in mitotic nuclei (Fig. 1C, lower row).

BNFA is a novel protein that physically interacts with NUDF in *A. nidulans*. Since several aspects of NUDF localization and the regulation of its activity are still unclear, we searched for additional, unknown interaction partners of NUDF and performed TAP using an nTAP*-tagged NUDF. The use of this tag allowed two subsequent affinity purifications, the first on IgG Sepharose due to the presence of two protein A domains and a second on calmodulin resin in the presence of Ca^{2+} by virtue of a calmodulin binding epitope (CBP) directly N terminal to NUDF. Both tags were separated by a TEV cleavage site so that CBP-NUDF could be cleaved off the first matrix by incubation with TEV protease. Elution from the calmodulin beads was achieved through titrating out calcium by the addition of EGTA.

The fusion protein was expressed from the authentic *nudF* promoter by the reintegration of the *nTAP**::*nudF* fusion (AGB249) into the *nudF* locus of a Δ*nudF* strain (AGB257). The functionality of the fusion protein was confirmed by its complementation of the nuclear migration and growth defect

of the *nudF* deletion (Fig. 3A). DAPI staining of nuclei showed that the even distribution of nuclei along hyphae was restored in the transformed strain AGB249, although a few nuclei accumulated in the remainder of the conidia. Nevertheless, the nearly full functionality of the fusion protein enabled this strain to grow like the parental strain AGB152 (wild-type *nudF*).

A. nidulans crude extracts were prepared from 18-h-old vegetative mycelia. The TAP was monitored by taking samples at critical steps of the procedure and detecting the NUDF fusion protein with an anti-CBP antibody in a Western hybridization (Fig. 3B). Proteins in the final eluate that bound to the IgG and calmodulin matrices, respectively, were analyzed by SDS-PAGE and silver staining (Fig. 3C). Proteins binding unspecifically to the beads could be identified by TAP using the crude extract of the parental strain AGB152, which did not express a *tap** fusion but instead expressed native *nudF* (Fig. 3C). Several high-molecular-weight proteins were present in both crude extracts, indicating that they were not copurified with NUDF but bound to the beads directly. The lower three bands in the lane with proteins from strain AGB249 were cut out and analyzed by tandem mass spectrometry after trypsin digestion. The upper band was identified as NUDF (AN6197.1; two tryptic peptides of the protein with cross correlation [Xcorr] values of 3.5 and 3.9) and the band below as the elongation factor 1A α-subunit (AN4218.1; three peptides with Xcorr values of 2.3, 3.0, and 3.4). The elongation factor also was identified in other control purifications, and since it was shown to bind to calmodulin (11), its copurification in this experiment probably was not due to a specific binding to NUDF. The lower band contained the gene product of ORF AN3213.1 (only one peptide, with an Xcorr value of 2.8), which we called BNFA.

BLAST analyses showed that BNFA did not bear similarities to any known protein. Therefore, manual annotation regarding the AN3213 locus and its neighboring loci (AN3211, AN3212, and AN3214) was performed using the genomes of *Aspergillus fumigatus*, *Aspergillus oryzae*, *Aspergillus terreus*, *Aspergillus niger*, and *Aspergillus flavus*. A BLAST search of the *A. niger* genome identified locus 669910-670782 on scaffold 8 (protein identity 41676). The encoded protein bears 27% identity and 53% similarity to BNFA, indicating a divergent protein even in closely related species. The syntheny of this genomic region was confirmed by the identification of genes homologous to AN3212.3 and AN3211.3, respectively, on scaffold 8 (loci 672614 to 673576 and 674136 to 674961). In the other *Aspergillus* species, no *bnfA* homolog could be detected. In *A. terreus*, the genes homologous to AN3212.3 and AN3211.3 were located next to each other (ATEG_07921.1 and ATEG_07922.1). In *A. fumigatus*, four other genes were inserted between the genes homologous to AN3212.3 and AN3214.3 (Afu4g01060-30), and in *A. oryzae* and *A. flavus* the neighboring loci were scattered along the genome. Thus, not only is BNFA a divergent protein but also the whole genomic region is highly variable. Therefore, BNFA presumably exists but still is untraceable in other organisms.

Domain analyses of BNFA indicated the presence of proline-rich regions spanning aa 11 to 85 and 238 to 297 and a C-terminal coiled-coil region between aa 302 and 350 (Fig. 4). The similar hypothetical protein of *A. niger* also was predicted to form a C-terminal coiled-coil region (aa 250 to 287), but it showed gaps in the proline-rich regions of BNFA. The strongest similarities between BNFA and the hypothetical *A. niger* protein were found in the central part located between these regions.

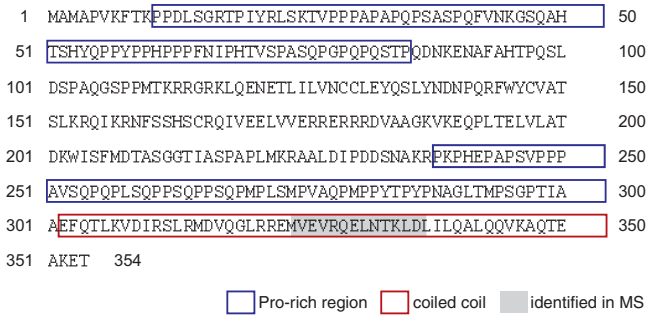

FIG. 4. *A. nidulans* BNFA protein sequence. BNFA (AN3213.3) contains two predicted proline-rich regions and a predicted C-terminal coiled-coil structure. One C-terminal peptide was identified by mass spectrometry (MS) after copurification with NUDF. The central part comprising aa 112 to 239 showed strong similarities to a hypothetical protein of *A. niger*.

The novel physical interaction of NUDF with BNFA in *A. nidulans* was confirmed genetically by yeast two-hybrid analysis. According to the genome sequence, in which there is no intron, a 1,065-bp coding sequence could be PCR amplified for *bnfA* from the cDNA library pCNS4 and was cloned into yeast two-hybrid vectors containing ORFs for the B42 activation domain and the LexA DNA-binding protein. The known interaction between NUDF and the coiled coil of NUDE was used as a positive control. The *b42-bnfA* fusion impaired the growth of *S. cerevisiae* strain EGY48 (data not shown), so the test for leucine prototrophy could not be performed. However, *lacZ* reporter gene expression was induced in EGY48 harboring the *b42-bnfA* fusion plus a *lexA-nudF* fusion, confirming the interaction between NUDF and BNFA (Fig. 3D). The expression of a *lexA-bnfA* fusion did not result in retarded growth (data not shown), and no interaction with B42-NUDF was observed in the β-galactosidase assay (Fig. 3D) due to the fact that this fusion protein was not properly expressed. No fusion protein was detected by Western hybridization (data not shown).

BNFA is located at *A. nidulans* SPBs in a NUDF-dependent manner. We deleted *bnfA* in order to investigate the cellular function of this novel protein. In the Δ*nkuA* strain A1149 and in AGB152, the *bnfA* ORF was replaced by the *zeo*::*pyrG*::*zeo* blaster cassette with subsequent counterselection against *pyrG*. However, no nuclear migration phenotype was observed. DAPI staining of nuclei in germinating hyphae demonstrated an even distribution, and in growth assays a wild-type-like growth rate and asexual development were observed in both strain backgrounds (data not shown).

A *gfp2-5*::*bnfA* fusion was expressed in the Δ*bnfA* strain AGB296 to gain insight into BNFA's cellular role through localization experiments. Again, a prominent nuclear dot pattern was observed in germinating hyphae characteristic of SPB proteins (Fig. 5A). In addition, a faint fluorescence was detected throughout the nuclei, which could indicate a role for BNFA in the nucleus, but it also might be caused by the rather

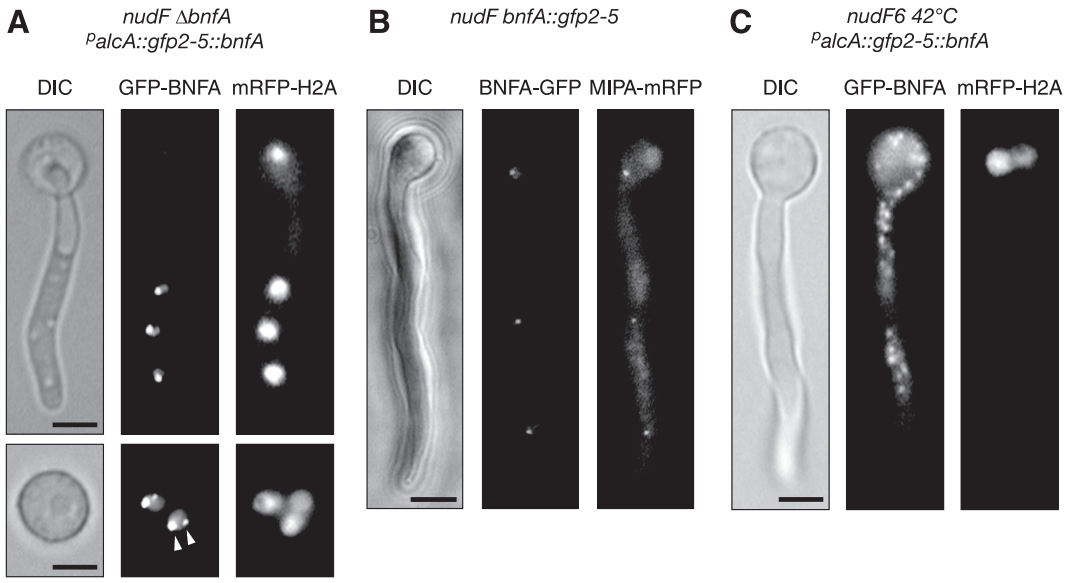

FIG. 5. BNFA is localized to *A. nidulans* SPBs in a NUDF-dependent manner. (A) Strain AGB297 (*nudF* Δ*bnfA* ^{p}*alcA*::*gfp2-5*::*bnfA*) was grown on MM containing 2% glycerol at room temperature overnight. GFP-BNFA was localized in small amounts throughout the nucleus but accumulated at SPBs during interphase (upper) and mitosis (lower). Arrowheads indicate two adjacent SPBs after duplication at the beginning of mitosis, when GFP-BNFA is not yet localized to the same extent to the new SPB as to the old one. Scale bars, 5 μm. (B) Strain AGB337 (*nudF bnfA*::*gfp2-5*) was grown on glucose-containing MM at room temperature overnight and showed the same nuclear dot pattern as that of the SPB-protein γ-tubulin (MIPA). Scale bar, 5 μm. (C) Strain AGB298 (*nudF6* ^{p}*alcA*::*gfp2-5*::*bnfA*) was incubated in MM containing 2% glycerol at 42°C for 8 h and showed widely distributed GFP-BNFA dots along the hypha in the absence of NUDF. Scale bar, 5 μm. DIC, differential interference contrast.

high expression from the *alcA* promoter during growth on glycerol-containing medium. As a control, nuclei were counterstained by the expression of an *mrfp*::*h2A* fusion (Fig. 5A). In several cases, we observed two dots of GFP-BNFA in close proximity to each other, indicating that the respective nuclei were undergoing mitosis, during which the SPB was duplicated for spindle formation (Fig. 5A). For clarification, a *bnfA*::*gfp2-5* fusion was expressed from the *bnfA* promoter in a strain with labeled SPBs (AGB337). Microscopy revealed the same fluorescent pattern within the cells, which was weaker due to the lower expression level, but it also corresponded to the γ-tubulin pattern. Again, an additional faint fluorescence was observed throughout nuclei, so that an overexpression effect could be ruled out.

Thus, BNFA could be detected at SPBs at different stages of the cell cycle. This result corroborated the NUDF-BNFA interaction, since YFP-NUDF also was localized to SPBs, albeit only during mitosis (35). These findings lead to the question of whether NUDC also interacted with BNFA. However, no association between the LexA-NUDC and B42-BNFA fusion proteins could be detected in a yeast two-hybrid assay (data not shown).

BNFA might be an integral part of the SPB recruiting NUDF to the nucleus, or BNFA might be placed at the SPB by means of NUDF. Therefore, GFP-NUDF was localized in the Δ*bnfA* strain and compared to the wild-type *bnfA* background (AGB300 and AGB301) to discriminate between these possibilities. GFP-NUDF was localized at MT plus ends during interphase and at the poles of mitotic nuclei, indicating that BNFA is not necessary for recruiting NUDF to SPBs (data not shown). The GFP-BNFA localization then was analyzed in the absence of NUDF. The *gfp2-5*::*bnfA* and *mrfp*::*h2A* fusions were expressed in a temperature-sensitive *nudF6* strain (AGB298), and fluorescence microscopy was performed after growth in glycerol-containing medium at room temperature and 42°C, respectively. At low temperature, GFP-BNFA localized to SPBs as seen before (data not shown). At 42°C, the typical nuclear migration defect could be observed with nuclei clustering in the spore, indicating the inactivity of NUDF. In this case, the GFP-BNFA signals were only rarely detected in the vicinity of nuclei, but discrete dots were dispersed throughout the hyphae (Fig. 5B). The same cytoplasmic clustering arose in the *nudF* deletion strain (AGB299), in which definitively no NUDF was present (data not shown). This observation showed that NUDF is required for positioning BNFA at SPBs.

DISCUSSION

In this study, we localized fungal NUDC and described its association with NUDF at SPBs and at the cortex. We identified BNFA as a novel NUDF binding protein that is localized at SPBs through its interaction with NUDF. These results lead to the following conclusions. (i) As seen from BiFC and BNFA localization experiments, NUDF is localized at SPBs not only during mitosis but also during interphase, although its amount there obviously is much smaller than that at the plus-end reservoir. (ii) In addition to its cortical localization, fungal NUDC binds NUDF in the cytoplasm and at SPBs at different stages of the cell cycle, showing that *A. nidulans* might also serve as a model organism for the analysis of mitotic NUDC functions. (iii) There must be a difference between the NUDF subsets at

MT plus ends and at SPBs, because neither BNFA nor NUDC was found at MT plus ends, where the amount of NUDF is especially high. (iv) At least at SPBs, the dynein/NUDF complex contains more proteins than assumed until now, as we have shown by copurifying BNFA.

The dynein regulatory complex at SPBs. In *Aspergillus*, NUDF was previously found at the poles of spindles of various lengths, but it was not directly observed there during interphase (35). NUDA was localized there only late during mitosis, for which NUDF was required, among others. Thus, it is not unlikely that small amounts of NUDF also are present there during interphase but could not yet be detected. Using BiFC microscopy, we obtained data indicating that NUDF is present at SPBs at different stages of the cell cycle. In addition, by means of analyzing the presence or absence of the NUDF binding protein BNFA at SPBs in the presence or absence of NUDF, a subset of NUDF could be indirectly localized there during interphase. NUDF's homolog LIS1, together with dynein, was shown to be necessary for coupling the centrosome to the nucleus in mammalian neurons and *Dictyostelium* (44, 52). LIS1 also was found there throughout the cell cycle, and this localization was not MT dependent in *Dictyostelium*, in contrast to the case for neurons. Therefore, LIS1 was suggested to be an integral centrosome component. The SPB of filamentous fungi differs from the centrosome in that it is embedded in the nuclear envelope. However, this difference does not obviously influence NUDF/LIS1 localization at this MT-organizing center. NUDF was shown to be positioned at spindle poles in the absence of dynein or MTs (35), and it seems likely that NUDE and CLIPA also are the NUDF anchors at SPBs. Mouse NUDE binds to six centrosomal proteins and is important for MT organization (17), and human Nude1 was described to be necessary for centrosomal LIS1 localization and MT nucleation (23). These results indicate an important recruiting function of NUDE and argue against NUDF/LIS being an SPB/centrosome component.

In our experiments, BNFA was seen only at SPBs and not on MTs or at their plus ends, where there is an abundant supply of NUDF. Therefore, we conclude that BNFA is recruited directly to SPBs by NUDF independently of dynein or MTs. Other anchors for BNFA seem unlikely, since the depletion of NUDF was sufficient to displace BNFA from SPBs. The expression of *bnfA-gfp* and *mipA*::*mrfp* in a *nudF6* or *nudF*Δ strain could further confirm the NUDF-dependent localization of BNFA to SPBs. Our observation also makes it unlikely that BNFA is an integral component of the SPB. At present it remains unknown if the NUDF complex is bound to the inner plate or outer plate of SPBs, but BNFA localization within the nucleus indicates binding to both sides of SPBs.

Furthermore, the data presented here indicate that fungal NUDC also is part of the dynein/NUDF complex at SPBs, which suggests that, in *A. nidulans*, NUDC also is involved in MT organization for nuclear migration and spindle formation. In our BiFC study, the NUDF-NUDC interaction was observed in the cytoplasm in addition to SPBs. This localization could be a functional association, or it could be due to the overexpression of the fusion proteins. Overexpression studies of NUDA and NUDE fusions, respectively, showed that in addition to the authentic comets at MT plus ends, immobile cytoplasmic specks also appeared, which were assumed to be artifacts (12). Therefore, we conclude that the SPB localization of NUDC, like that of NUDF, is authentic and due to a specific function at this location, whereas the cytoplasmic localization is an artifact; however, at the moment we cannot rule out that it also is significant.

At present, is remains unclear how NUDC is attached to the SPB or the cortex. NUDF might be at least partly responsible for NUDC localization, but the opposite could be true as well. The colocalization of hNUDC with MTs could indicate direct MT binding (42), but it also is possible that NUDC binds to integral SPB components, other dynein complex subunits like NUDE, or additional regulatory proteins. Therefore, a screening for proteins binding to NUDC or to BNFA will be a target of our future research to confirm these localization studies and to clarify the molecular function of the dynein regulatory complex at this MT-organizing center.

Different subsets of NUDF and NUDC. The colocalization of NUDF and BNFA at SPBs, but not MT plus ends, suggests the existence of different subsets of NUDF. Similarly, there might be a difference between the NUDC population at the cortex and the NUDC associated with NUDF at SPBs. At SPBs, important regulatory mechanisms perform functions. Mitotic kinases and phosphatases like NIMA, PLKA, and BIMG are located there in *A. nidulans* and control mitotic events through phosphorylation/dephosphorylation cascades (2, 9, 19). LIS1 is a phosphoprotein (47), and NUDF was shown to be modified (our unpublished data). This raises the possibility that NUDF is phosphorylated at SPBs and therefore associates with specific proteins, like BNFA, at this site but not at others. The described phosphorylation of hNUDC by PLK1 (65) suggests that fungal NUDC also is phosphorylated. hNUDC was shown to bind PLK1, and upon its phosphorylation by PLK1 it associates with kinetochores (41). A similar mechanism also may apply to NUDC in *Aspergillus*. It will be very interesting to investigate if the phosphorylation of these nuclear migration proteins is a means to control the associations with specific factors, which in turn account for the different functions of dynein during the cell cycle.

The dynein/LIS1 complex contains more proteins than previously known. The determination of protein structures and multiple interaction studies lead to a model for LIS1 interaction with Ndel1 and dynein proposed by Tarricone et al., in which LIS1 dimerizes via its LisH domain and interacts with a Nudel dimer through the coiled-coil helix (53). In addition, the LisH domains of LIS1 contact the dynein heavy-chain stems, while the WD40 domains reside near the first AAA domain of the heavy-chain heads. In this study, we showed that fungal NUDC can associate with NUDF/LIS1, too, and that it can bind to NUDF's WD40 domain, which is in agreement with the described structural model, because the WD40 domains seem accessible to additional binding partners. How BNFA is incorporated in this complex is unknown, but it might bind NUDF's coiled-coil helix via its own C-terminal helix or might also contact the WD40 domain. In our two-hybrid analyses, BNFA did not bind to NUDC, which argues against the latter possibility, but BNFA is able to dimerize and therefore might also form heterodimers with other coiled-coil proteins (our unpublished results).

Here, we showed that there is at least one additional protein that is specifically recruited by NUDF to the dynein complex at

SPBs. The function of BNFA in the dynein/NUDF complex, the existence of homologous genes, and which other proteins might assume its role in other organisms remains to be elucidated. The continuous improvement of genome annotations might complete the search for yet-undiscovered proteins in other organisms. On the other hand, it cannot be excluded that BNFA remains unique to fungi. For another formerly unique SPB-associated protein, SNAD, which affects septation in *A. nidulans* (36), analogous proteins now can be found in other fungi. Similarly, the SPB protein APSB seems to be required for MT organization only in fungi (56). Thus, given the slight difference between the SPB of fungi and the centrosome of higher eukaryotes, there could be a difference in dynein function or MT organization at these sites that involves BNFA. It is an interesting goal for future research to decipher BNFA's molecular function and identify analogous proteins in higher eukaryotes.

ACKNOWLEDGMENTS

We thank Gabriele Heinrich and Verena Pretz for excellent technical assistance. We are indebted to Sven Krappmann for providing the knockout blaster cassette for *Aspergillus*, the cDNA library, and the mRFP-H2A marker module. We thank Xin Xiang for sending us the CFP-H2A marker plasmid and strain XX20, Berl R. Oakley for providing the *Aspergillus* Δ*nkuA* strain, and Reinhard Fischer for pMCB17apx and the EYFP plasmids.

This work was supported by the Deutsche Forschungsgemeinschaft (DFG) through the DFG Research Center for Molecular Physiology of the Brain (CMPB) and by grants from the Volkswagen-Stiftung and the Fonds der Chemischen Industrie.

REFERENCES

1. **Aumais, J. P., S. N. Williams, W. Luo, M. Nishino, K. A. Caldwell, G. A. Caldwell, S. H. Lin, and L. Y. Yu-Lee.** 2003. Role for NudC, a dynein-associated nuclear movement protein, in mitosis and cytokinesis. J. Cell Sci. **116:**1991–2003.
2. **Bachewich, C., K. Masker, and S. Osmani.** 2005. The polo-like kinase PLKA is required for initiation and progression through mitosis in the filamentous fungus *Aspergillus nidulans*. Mol. Microbiol. **55:**572–587.
3. **Blum, H., H. Beier, and H. J. Gross.** 1987. Improved silver staining of plant proteins, RNA and DNA in polyacrylamide gels. Electrophoresis **8:**93–99.
4. **Blumenstein, A., K. Vienken, R. Tasler, J. Purschwitz, D. Veith, N. Frankenberg-Dinkel, and R. Fischer.** 2005. The *Aspergillus nidulans* phytochrome FphA represses sexual development in red light. Curr. Biol. **15:**1833–1838.
5. **Busch, S., S. E. Eckert, S. Krappmann, and G. H. Braus.** 2003. The COP9 signalosome is an essential regulator of development in the filamentous fungus *Aspergillus nidulans*. Mol. Microbiol. **49:**717–730.
6. **Busch, S., E. U. Schwier, K. Nahlik, Ö. Bayram, K. Helmstaedt, O. W. Draht, S. Krappmann, O. Valerius, W. N. Lipscomb, and G. H. Braus.** 2007. An eight-subunit COP9 signalosome with an intact JAMM motif is required for fungal fruit body formation. Proc. Natl. Acad. Sci. USA **104:**8089–8094.
7. **Chaveroche, M., J. Ghigo, and C. d'Enfert.** 2000. A rapid method for efficient gene replacement in the filamentous fungus Aspergillus nidulans. Nucleic Acids Res. **28:**E97.
8. **Chiu, Y. H., X. Xiang, A. L. Dawe, and N. R. Morris.** 1997. Deletion of *nudC*, a nuclear migration gene of *Aspergillus nidulans*, causes morphological and cell wall abnormalities and is lethal. Mol. Biol. Cell **8:**1735–1749.
9. **De Souza, C. P., A. H. Osmani, L. P. Wu, J. L. Spotts, and S. A. Osmani.** 2000. Mitotic histone H3 phosphorylation by the NIMA kinase in *Aspergillus nidulans*. Cell **102:**293–302.
10. **Dobyns, W. B., O. Reiner, R. Carrozzo, and D. H. Ledbetter.** 1993. Lissencephaly. A human brain malformation associated with deletion of the *LIS1* gene located at chromosome 17p13. JAMA **270:**2838–2842.
11. **Durso, N. A., and R. J. Cyr.** 1994. A calmodulin-sensitive interaction between MTs and a higher plant homolog of elongation factor-1 alpha. Plant Cell **6:**893–905.
12. **Efimov, V. P.** 2003. Roles of NUDE and NUDF proteins of *Aspergillus nidulans*: insights from intracellular localization and overexpression effects. Mol. Biol. Cell **14:**871–888.
13. **Efimov, V. P., and N. R. Morris.** 2000. The LIS1-related NUDF protein of *Aspergillus nidulans* interacts with the coiled-coil domain of the NUDE/RO11 protein. J. Cell Biol. **150:**681–688.
14. **Efimov, V. P., J. Zhang, and X. Xiang.** 2006. CLIP-170 homologue and NUDE play overlapping roles in NUDF localization in *Aspergillus nidulans*. Mol. Biol. Cell **17:**2021–2034.
15. **Elble, R.** 1992. A simple and efficient procedure for transformation of yeasts. BioTechniques **13:**18–20.
16. **Faulkner, N. E., D. L. Dujardin, C. Y. Tai, K. T. Vaughan, C. B. O'Connell, Y. Wang, and R. B. Vallee.** 2000. A role for the lissencephaly gene *LIS1* in mitosis and cytoplasmic dynein function. Nat. Cell Biol. **2:**784–791.
17. **Feng, Y., E. C. Olson, P. T. Stukenberg, L. A. Flanagan, M. W. Kirschner, and C. A. Walsh.** 2000. LIS1 regulates CNS lamination by interacting with mNudE, a central component of the centrosome. Neuron **28:**665–679.
18. **Fernández-Ábalos, J. M., H. Fox, C. Pitt, B. Wells, and J. H. Doonan.** 1998. Plant-adapted green fluorescent protein is a versatile vital reporter for gene expression, protein localization and mitosis in the filamentous fungus Aspergillus nidulans. Mol. Microbiol. **27:**121–130.
19. **Fox, H., P. C. Hickey, J. M. Fernández-Ábalos, P. Lunness, N. D. Read, and J. H. Doonan.** 2002. Dynamic distribution of $BIMG^{PP1}$ in living hyphae of *Aspergillus nidulans* indicates a novel role in septum formation. Mol. Microbiol. **45:**1219–1230.
20. **Fukata, M., T. Watanabe, J. Noritake, M. Nakagawa, M. Yamaga, S. Kuroda, Y. Matsuura, A. Iwamatsu, F. Perez, and K. Kaibuchi.** 2002. Rac1 and Cdc42 capture microtubules through IQGAP1 and CLIP-170. Cell **109:**873–885.
21. **Garcia-Ranea, J. A., G. Mirey, J. Camonis, and A. Valencia.** 2002. p23 and HSP20/alpha-crystallin proteins define a conserved sequence domain present in other eukaryotic protein families. FEBS Lett. **529:**162–167.
22. **Golemis, E., I. Serebriiskii, R. Finley, Jr., M. Kolonin, J. Gyuris, and R. Brent.** 1999. Interaction trap/two-hybrid system to identify interacting proteins, p. 20.1.1–20.1.40. *In* F. M. Ausubel, R. Brent, R. E. Kingston, D. D. Moore, J. G. Seidmann, A. J. Smith, and K. Struhl (ed.), Current protocols in molecular biology. John Wiley & Sons, Inc., New York, NY.
23. **Guo, J., Z. Yang, W. Song, Q. Chen, F. Wang, Q. Zhang, and X. Zhu.** 2006. Nudel contributes to microtubule anchoring at the mother centriole and is involved in both dynein-dependent and -independent centrosomal protein assembly. Mol. Biol. Cell **17:**680–689.
24. **Guthrie, C., and G. Fink.** 1991. Guide to yeast genetics and molecular biology. Methods Enzymol. **194:**15.
25. **Hoff, B., and U. Kück.** 2005. Use of bimolecular fluorescence complementation to demonstrate transcription factor interaction in nuclei of living cells from the filamentous fungus *Acremonium chrysogenum*. Curr. Genet. **47:**132–138.
26. **Hoppert, M., and A. Holzenburg.** 1998. Electron microscopy in microbiology, p. 48. Bios Scientific, Oxford, United Kingdom.
27. **Inoue, H., H. Nojima, and H. Okayama.** 1990. High efficiency transformation of *Escherichia coli* with plasmids. Gene **96:**23–28.
28. **Käfer, E.** 1977. Meiotic and mitotic recombination in *Aspergillus* and its chromosomal aberrations. Adv. Genet. **19:**33–131.
29. **Kim, M. H., D. R. Cooper, A. Oleksy, Y. Devedjiev, U. Derewenda, O. Reiner, J. Otlewski, and Z. S. Derewenda.** 2004. The structure of the N-terminal domain of the product of the lissencephaly gene *Lis1* and its functional implications. Structure **12:**987–998.
30. **Kolar, M., P. J. Punt, C. A. van den Hondel, and H. Schwab.** 1988. Transformation of *Penicillium chrysogenum* using dominant selection markers and expression of an *Escherichia coli lacZ* fusion gene. Gene **62:**127–134.
31. **Komarova, Y. A., A. S. Akhmanova, S. Kojima, N. Galjart, and G. G. Borisy.** 2002. Cytoplasmic linker proteins promote microtubule rescue in vivo. J. Cell Biol. **159:**589–599.
32. **Krappmann, S., and G. H. Braus.** 2003. Deletion of *Aspergillus nidulans aroC* using a novel blaster module that combines ET cloning and marker rescue. Mol. Genet. Genomics **268:**675–683.
33. **Krappmann, S., N. Jung, B. Medic, S. Busch, R. A. Prade, and G. H. Braus.** 2006. The *Aspergillus nidulans* F-box protein GrrA links SCF activity to meiosis. Mol. Microbiol. **61:**76–88.
34. **Laemmli, U. K.** 1970. Cleavage of structural proteins during the assembly of the head of bacteriophage T4. Nature **227:**680–685.
35. **Li, S., C. E. Oakley, G. Chen, X. Han, B. R. Oakley, and X. Xiang.** 2005. Cytoplasmic dynein's mitotic spindle pole localization requires a functional anaphase-promoting complex, gamma-tubulin, and NUDF/LIS1 in *Aspergillus nidulans*. Mol. Biol. Cell **16:**3591–3605.
36. **Liu, B., and N. R. Morris.** 2000. A spindle pole body-associated protein, SNAD, affects septation and conidiation in *Aspergillus nidulans*. Mol. Gen. Genet. **263:**375–387.
37. **Morris, N. R.** 2000. Nuclear migration. From fungi to the mammalian brain. J. Cell Biol. **148:**1097–1101.
38. **Morris, S. M., U. Albrecht, O. Reiner, G. Eichele, and L. Y. Yu-Lee.** 1998. The lissencephaly gene product Lis1, a protein involved in neuronal migration, interacts with a nuclear movement protein, NudC. Curr. Biol. **8:**603–606.
39. **Morris, S. M., and L. Y. Yu-Lee.** 1998. Expression of RNUDC, a potential nuclear movement protein, in mammalian cells: localization to the Golgi apparatus. Exp. Cell Res. **238:**23–32.
40. **Nayak, T., E. Szewczyk, C. E. Oakley, A. Osmani, L. Ukil, S. L. Murray, M. J.**

Hynes, S. A. Osmani, and B. R. Oakley. 2006. A versatile and efficient gene-targeting system for *Aspergillus nidulans*. Genetics **172:**1557–1566.
41. **Nishino, M., Y. Kurasawa, R. Evans, S. H. Lin, B. R. Brinkley, and L. Y. Yu-Lee.** 2006. NudC is required for Plk1 targeting to the kinetochore and chromosome congression. Curr. Biol. **16:**1414–1421.
42. **Pan, R. M., Y. Yang, M. X. Wei, X. B. Yu, Y. C. Ge, and P. Xu.** 2005. A microtubule associated protein (hNUDC) binds to the extracellular domain of thrombopoietin receptor (Mpl). J. Cell Biochem. **96:**741–750.
43. **Punt, P. J., and C. A. van den Hondel.** 1992. Transformation of filamentous fungi based on hygromycin B and phleomycin resistance markers. Methods Enzymol. **216:**447–457.
44. **Rehberg, M., J. Kleylein-Sohn, J. Faix, T. H. Ho, I. Schulz, and R. Graf.** 2005. *Dictyostelium* LIS1 is a centrosomal protein required for microtubule/cell cortex interactions, nucleus/centrosome linkage, and actin dynamics. Mol. Biol. Cell **16:**2759–2771.
45. **Reiner, O., S. Sapoznik, and T. Sapir.** 2006. Lissencephaly 1 linking to multiple diseases: mental retardation, neurodegeneration, schizophrenia, male sterility, and more. Neuromol. Med. **8:**547–566.
46. **Roth, J., M. Bendayan, E. Carlemalm, W. Villiger, and M. Garavito.** 1981. Enhancement of structural preservation and immunocytochemical staining in low temperature embedded pancreatic tissue. J. Histochem. Cytochem. **29:**663–671.
47. **Sapir, T., A. Cahana, R. Seger, S. Nekhai, and O. Reiner.** 1999. LIS1 is a microtubule-associated phosphoprotein. Eur. J. Biochem. **265:**181–188.
48. **Sasaki, S., A. Shionoya, M. Ishida, M. J. Gambello, J. Yingling, A. Wynshaw-Boris, and S. Hirotsune.** 2000. A LIS1/NUDEL/cytoplasmic dynein heavy chain complex in the developing and adult nervous system. Neuron **28:**681–696.
49. **Shevchenko, A., M. Wilm, O. Vorm, and M. Mann.** 1996. Mass spectrometric sequencing of proteins silver-stained polyacrylamide gels. Anal. Chem. **68:**850–858.
50. **Song, S., T. Zhang, W. Qi, W. Zhao, B. Xu, and J. Liu.** 1993. Transformation of *Escherichia coli* with foreign DNA by electroporation. Chin. J. Biotechnol. **9:**197–201.
51. **Southern, E. M.** 1975. Detection of specific sequences among DNA fragments separated by gel electrophoresis. J. Mol. Biol. **98:**503–517.
51a. **Su, W., S. Li, B. R. Oakley, and X. Xiang.** 2004. Dual-color imaging of nuclear division and mitotic spindle elongation in live cells of *Aspergillus nidulans*. Eukaryot. Cell **3:**553–556.
52. **Tanaka, T., F. F. Serneo, C. Higgins, M. J. Gambello, A. Wynshaw-Boris, and J. G. Gleeson.** 2004. Lis1 and doublecortin function with dynein to mediate coupling of the nucleus to the centrosome in neuronal migration. J. Cell Biol. **165:**709–721.
53. **Tarricone, C., F. Perrina, S. Monzani, L. Massimiliano, M. H. Kim, Z. S. Derewenda, S. Knapp, L. H. Tsai, and A. Musacchio.** 2004. Coupling PAF signaling to dynein regulation: structure of LIS1 in complex with PAF-acetylhydrolase. Neuron **44:**809–821.
54. **Tesfaigzi, J., W. Smith-Harrison, and D. M. Carlson.** 1994. A simple method for reusing Western blots on PVDF membranes. BioTechniques **17:**268–269.
55. **Vallee, R. B., and J. W. Tsai.** 2006. The cellular roles of the lissencephaly gene LIS1, and what they tell us about brain development. Genes Dev. **20:**1384–1393.
56. **Veith, D., N. Scherr, V. P. Efimov, and R. Fischer.** 2005. Role of the spindle-pole-body protein ApsB and the cortex protein ApsA in microtubule organization and nuclear migration in *Aspergillus nidulans*. J. Cell Sci. **118:**3705–3716.
57. **Willins, D. A., B. Liu, X. Xiang, and N. R. Morris.** 1997. Mutations in the heavy chain of cytoplasmic dynein suppress the *nudF* nuclear migration mutation of *Aspergillus nidulans*. Mol. Gen. Genet. **255:**194–200.
58. **Willins, D. A., X. Xiang, and N. R. Morris.** 1995. An alpha tubulin mutation suppresses nuclear migration mutations in *Aspergillus nidulans*. Genetics **141:**1287–1298.
59. **Woodcock, D. M., P. J. Crowther, J. Doherty, S. Jefferson, E. DeCruz, M. Noyer-Weidner, S. S. Smith, M. Z. Michael, and M. W. Graham.** 1989. Quantitative evaluation of *Escherichia coli* host strains for tolerance to cytosine methylation in plasmid and phage recombinants. Nucleic Acids Res. **17:**3469–3478.
60. **Xiang, X., S. M. Beckwith, and N. R. Morris.** 1994. Cytoplasmic dynein is involved in nuclear migration in *Aspergillus nidulans*. Proc. Natl. Acad. Sci. USA **91:**2100–2104.
61. **Xiang, X., A. H. Osmani, S. A. Osmani, M. Xin, and N. R. Morris.** 1995. NudF, a nuclear migration gene in *Aspergillus nidulans*, is similar to the human LIS-1 gene required for neuronal migration. Mol. Biol. Cell **6:**297–310.
62. **Yang, L., L. Ukil, A. Osmani, F. Nahm, J. Davies, C. P. De Souza, X. Dou, A. Perez-Balaguer, and S. A. Osmani.** 2004. Rapid production of gene replacement constructs and generation of a green fluorescent protein-tagged centromeric marker in *Aspergillus nidulans*. Eukaryot. Cell **3:**1359–1362.
63. **Zhang, J., S. Li, R. Fischer, and X. Xiang.** 2003. Accumulation of cytoplasmic dynein and dynactin at microtubule plus ends in *Aspergillus nidulans* is kinesin dependent. Mol. Biol. Cell **14:**1479–1488.
64. **Zhang, M. Y., N. N. Huang, G. A. Clawson, S. A. Osmani, W. Pan, P. Xin, M. S. Razzaque, and B. A. Miller.** 2002. Involvement of the fungal nuclear migration gene *nudC* human homolog in cell proliferation and mitotic spindle formation. Exp. Cell Res. **273:**73–84.
65. **Zhou, T., J. P. Aumais, X. Liu, L. Y. Yu-Lee, and R. L. Erikson.** 2003. A role for Plk1 phosphorylation of NudC in cytokinesis. Dev. Cell **5:**127–138.
66. **Zhuang, L., J. Zhang, and X. Xiang.** 2007. Point mutations in the stem region and the fourth AAA domain of cytoplasmic dynein heavy chain partially suppress the phenotype of NUDF/LIS1 loss in *Aspergillus nidulans*. Genetics **175:**1185–1196.